January 14, 2010

Analysis of Non-Covalent Interactions Between the Nanoparticulate Fillers and the Matrix Polymer as Applied to Shape Memory Performance

I. Sedat Gunes, *University of Akron Main Campus*
Cesar Perez-Bolivar, *Bowling Green State University - Main Campus*
Feina Cao, *Bowling Green State University - Main Campus*
Guillermo A. Jimenez, *University of Akron Main Campus*
Pavel Anzenbacher, *Bowling Green State University*, et al.

Analysis of non-covalent interactions between the nanoparticulate fillers and the matrix polymer as applied to shape memory performance†

I. Sedat Gunes,[a] César Pérez-Bolivar,[b] Feina Cao,‡[a] Guillermo A. Jimenez,§[a] Pavel Anzenbacher, Jr.[b] and Sadhan C. Jana*[a]

Received 21st October 2009, Accepted 19th December 2009
First published as an Advance Article on the web 14th January 2010
DOI: 10.1039/b922027e

Non-covalent interactions between filler particles and polyurethanes were investigated using fluorescence emission spectroscopy. The results were used in the analysis of shape memory (SM) performance of polyurethanes. Composites of shape memory polyurethane (SMPU) and carbon nanofiber (CNF), oxidized carbon nanofiber (ox-CNF), organoclay, silicon carbide, and carbon black were prepared from diphenylmethane diisocyanate, 1,4-butanediol, and poly(caprolactone)diol. It was revealed by fluorescence emission spectroscopy that primarily the urethane groups located in the hard segments of SMPU interacted with the polar functional groups on filler particles. A close correlation between the extent of non-covalent filler–matrix interactions, soft segment crystallinity, and SM properties of polyurethane composites was discussed. It was observed that weak non-covalent interactions of polymer chains with CNF and SiC particles caused significant reductions in soft segment crystallinity of SMPU and hence the shape memory properties of the composites.

1. Introduction

Shape memory polymers (SMPs) are capable of recovering their original shape from a deformed state upon application of an appropriate external stimulus, such as heat or exposure to solvent.[1,2] The majority of SMPs are rubberlike[2] with properties similar to conventional elastomers and rubbers. The entropic elasticity of deformed polymer network is responsible for shape memory properties of rubberlike SMPs. Some shape memory polymers, such as nematic elastomers and electroactive polymers, do not use entropic elasticity for shape recovery. These are defined as mesomorphic SMPs.[2] In this context, methods used for mechanical reinforcement of conventional elastomers, *e.g.*, by incorporating nanoscopic inorganic fillers, are also useful for improvement of shape memory properties of rubberlike SMPs. The magnitude of improvement, however, depends on the state of filler dispersion and the nature of filler–polymer interactions.[2]

Favorable filler–polymer interactions are essential in preparation of true nanocomposites and in realizing superior mechanical and thermal properties, as highlighted previously.[3,4] Filler–polymer interactions in composites can be broadly classified as formation of covalent bonds and non-covalent interactions.[5,6] Covalent bonds are formed between the reactive functional groups on filler particles and polymer chains. This may require long reaction time and exposure to high temperature and is often facilitated by carrying out such reactions in solutions.[7] On the other hand, non-covalent interactions between the polymer and the filler particles are easily produced at the time of composite preparation, usually without an additional processing step, or without the use of intermediate compounds. The most crucial step in attaining favorable non-covalent filler–polymer interactions for a given polymer system is the proper selection of the fillers and in some cases an appropriate method of chemical modification of the fillers.

The analysis of non-covalent filler–matrix interactions in polymer composites *via* spectroscopic methods, such as nuclear magnetic resonance (NMR), Fourier-transform infrared (FT-IR) spectroscopy, and fluorescence emission spectroscopy, can often be challenging.[8] For example, NMR offers significantly lower resolution for solid samples.[8] The inherently lower sensitivity of FT-IR is further compromised in the analysis of polymer composites filled with carbonaceous fillers capable of absorbing infrared (IR) radiation.[9] On the other hand, the fluorescence emission spectrometry method is known for its remarkably higher sensitivity and selectivity, even when applied to solid polymers filled with inorganic particles.[10] Besides the spectroscopic methods, rheological analysis was used to obtain evidence of favorable non-covalent filler–polymer interactions.[11] For example, favorable polar–polar interactions between polar fillers, such as mica, and a polar polymer, such as styrene–butadiene–styrene (SBS), were previously identified from the increase of melt viscosity.[11] However, rheological analysis is sometimes unwieldy, *e.g.*, when performed for composites with fillers dispersed at multiple length scales—such as microscopic, nanoscopic, or combinations or when fillers undergo substantial attrition of length, *e.g.*, in composites of glass and carbon fibers.

In this work, we analyzed the nature of filler–polymer interactions in composites of shape memory polyurethanes (SMPUs) filled with carbon nanofiber (CNF), oxidized carbon nanofiber (ox-CNF), organoclay, silicon carbide, and carbon black. Our

[a]*Department of Polymer Engineering, The University of Akron, Akron, OH, 44325, USA. E-mail: janas@uakron.edu; Fax: +1 330 258 2339; Tel: +1 330 972 8293*
[b]*Department of Chemistry and Center for Photochemical Sciences, Bowling Green State University, Bowling Green, OH, 43403, USA*
† This paper is part of a *Journal of Materials Chemistry* themed issue on Actively Moving Polymers. Guest editor: Andreas Lendlein.
‡ *Present address*: Lubrizol Advanced Materials, Inc., Avon Lake, OH 44141, USA.
§ *Present address*: Laboratory of Polymers (POLIUNA), School of Chemistry, Universidad Nacional, Heredia, 86-3000 Costa Rica.

earlier studies[4,6,12] suggested that ox-CNF particles dispersed much better than CNF in SMPU possibly due to favorable interactions between ox-CNF particles and polar SMPU. Gunes *et al.*[4,12] observed pronounced reduction in soft segment crystallinity in composites of CNF and SiC in SMPU, although it was not known *a priori* why such reduction took place. Note that reduction in soft segment crystallinity in composites of CNF and SiC also led to dramatic reduction in shape memory properties. It should be noted that SMPU used in this work was an alternating block copolymer of highly polar urethane hard segments and less polar ester-type soft segments. It was anticipated that the high selectivity and sensitivity of fluorescence emission spectroscopy[13] would present sufficient insight on the nature of interactions of different segments of SMPU with the filler particles. Specifically, we intended to establish which of hard and soft segments produced more interactions with the filler particles.

2. Experimental

2.1. Materials

SMPU with 33% hard segment was synthesized from diphenylmethane diisocyanate (MDI, Mondur®M, Bayer Material Science, Pittsburg, PA), 1,4-butanediol (BD, Avocado Organics, UK), and poly(caprolactone)diol (PCL-diol, Solvay Chemical, UK) of molecular weight 4000 g mol^{-1}. The ingredients were mixed in stoichiometric ratio of 6 : 5 : 1 by moles of MDI, BD, and PCL-diol respectively. A tin catalyst, DABCO T120 (Air Products, Allentown, PA), was used to expedite chain extension reactions. The soft segment of the resultant SMPU was found to be semi-crystalline with melting point of approximately 45 °C.

In addition, two model compounds, phenyl urethane (ethyl *N*-phenylcarbamate) and *N*-methyl urethane (ethyl *N*-methylcarbamate), were obtained from TCI America (Portland, OR). These compounds helped emulate the interactions of urethane groups with filler particles without interference from the soft segments of SMPU. The chemical structures of these compounds are presented in Fig. 1.

Vapor grown carbon nanofiber (CNF, Pyrograph III® PR-24-PS) and vapor grown oxidized carbon nanofiber (ox-CNF, Pyrograph III® PR-24-PS-ox) were obtained from Applied Sciences, Inc. (Cedarville, OH) with diameters ranging from 60–200 nm and lengths of 30–100 μm. Cloisite®30B, containing organic quaternary ammonium ions $N^+(CH_2CH_2OH)_2(CH_3)T$, where T represents an alkyl group with approximately 65% $C_{18}H_{37}$, 30% $C_{16}H_{33}$, and 5% $C_{14}H_{29}$, was obtained from Southern Clay Products (Gonzalez, TX). SiC was obtained in β-crystalline form (NanoSiC®) from MTI Corp. (Richmond, CA) with an average size smaller than 30 nm and a density of 3.22 g cm^{-3}. A high structure, conductive grade CB (Ketjenblack®EC 300J) was obtained from Akzo Nobel (Norcross, GA). This grade of CB offered a pore volume of 0.310–0.345 $\times$ 10^{-3} m^3 per 100 g as determined from dibutyl phthalate absorption.[14]

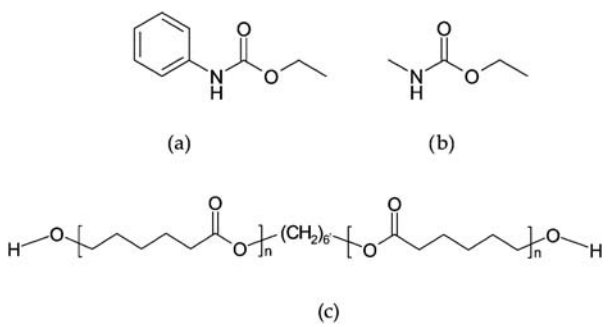

Fig. 1 Chemical structures of (a) phenyl urethane, (b) *N*-methyl urethane, (c) poly(caprolactone)diol (M_W = 4000 g mol^{-1}).

2.2. Preparation of composites

The composites of SMPU with CNF and ox-CNF were prepared in a low shear chaotic mixer.[6] It was observed that low shear rate of mixing, *e.g.*, 4.8 s^{-1} at the rotor wall and 2.7 s^{-1} at the mixing chamber, helped to preserve nanofiber length. In addition, the chaotic trajectory of the fluid improved both dispersive and distributive mixing.[6] Consequently, the composites produced in a chaotic mixer offered better mechanical and thermal properties, and electrical conductivity compared to materials prepared in commercial internal mixers under similar shear rates.[6] The shape memory polymer composites prepared in a chaotic mixer also provided much improved shape memory properties.[12] On the other hand, we found high shear internal mixers are more suitable for good filler dispersion in preparation of polymer composites of non-fibrous fillers, such as organoclay, SiC, and CB. Detailed information on mixing protocol and the effects of mixing time on product properties were reported for SMPU.[12] Optimum chaotic mixing parameters for urethane polymerization were also investigated.[15]

2.3. Characterization

The specimens with thickness of about 70 nm were microtomed under cryogenic conditions using a Reichert Ultracut S/FC S ultramicrotome (Leica, Germany) to obtain transmission electron microscopic (TEM) images with a JEOL TEM device (JEM 1200EXII) at120 kV. Thin slices (~50 to 70 μm thick) of specimens were analyzed using a Leitz Laborlux 12 Pol S optical microscope (OM) (Oberkochen, Germany) in transmission mode, and images were recorded with a digital camera (Diagnostic Instruments, Sterling Heights, MI). Fluorescence emission spectra were recorded on a single-photon-counting spectrofluorimeter (FL/FS 900, Edinburgh Analytical Instruments, Livingston, UK) equipped with a CW 450 W xenon arc lamp. The focal length for both excitation and emission monochromators was 300 mm. Both monochromators had a Czerny–Turner design triple grating turret. The resolution for the monochromators was 0.05 nm. The excitation wavelength was 266 nm. The detector was a single-photon-counting photomultiplier. The assignment of peak locations and corresponding fitting of fluorescence spectra were performed with curve fitting and data analysis software, Fityk 0.7.7¶.

3. Results and discussion

3.1. Filler surface properties and impact on filler dispersion

The states of filler dispersion in SMPU composites were analyzed earlier in detail in light of the nature of functional groups residing

¶ Fityk 0.7.7 is a free computer program which can be obtained from: http://www.unipress.waw.pl/fityk (September 9, 2009).

on the surfaces of filler particles.[4,12] It was identified using X-ray photoelectron spectroscopy (XPS) that the surfaces of ox-CNF and CB particles contained significant amounts of oxygen residing as polar functional groups. Also recall that the clay used in this work was an organically modified grade with about 32 wt% of organic surfactants.[16] The surface composition of SiC particles was found to be 60.8% carbon, 11.3% oxygen, and 27.9% silicon, all in mole percent, as determined by XPS. The oxygen containing polar functional groups on SiC were identified as O–C=O and COOH, which possibly originated from slow oxidation at room temperature of SiC molecules at the surface.[17] In view of this, one may imagine that SiC particles directly exposed to atmospheric oxygen during storage experienced such oxidation. The XPS data indicated that the surfaces of CNF particles were almost entirely composed of graphitic carbon and the presence of oxygen or oxygen-rich polar functional groups was insignificant.[6] The ox-CNF particles were produced by controlled oxidation of CNF in air, at 400–500 °C[18] and as a result oxygen-rich polar functional groups, such as C–O–C, C=O, –COOR, and –COOH, were generated on the surfaces, as revealed by XPS.[6] The XPS data indicated that the molar ratios of carbon atoms to oxygen atoms on the surfaces of CNF and ox-CNF were respectively 66.7 and 7.7.[6] Controlled oxidation also eliminated a significant portion of amorphous carbon present on the fibers[19] which in turn produced a relatively less entangled fiber morphology in as-received ox-CNFs (see Fig. 1 in ref. 6).

It was found using TEM images that organoclay and ox-CNF particles dispersed well in SMPU. On the other hand, micrometre-sized particle agglomerates were observed in composites of CNF and SiC (Fig. 2a and b). These observations suggested favorable non-covalent interactions in the composites of organoclay and ox-CNF considered in our earlier work, but FT-IR spectra of the composites did not present significant difference from that of the pristine SMPU and thermo-mechanical analyses of composites did not reveal distinguishable differences in glass transition temperature.[4] Microscopic agglomerates with an average size of 10 μm were found in the case of CB.[4] In some regions of the composites well-dispersed CB particles with an average size down to 100 nm were also observed, in line with earlier reports.[14]

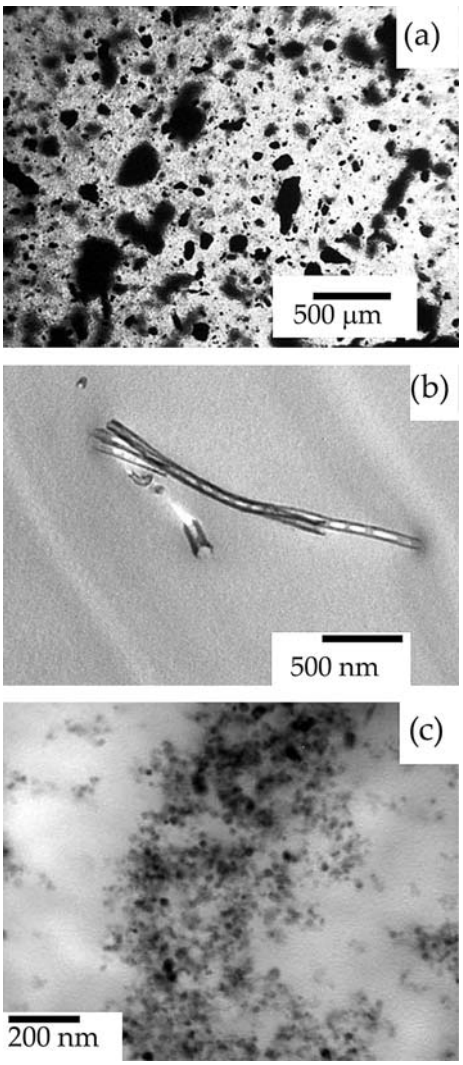

Fig. 2 Representative images showing the states of filler dispersion in CNF–SMPU and SiC–SMPU composites. (a) Optical microscope image of CNF–SMPU composite with 1 wt% filler content. The image was generated at low magnification in order to evaluate overall state of filler dispersion. (b) Transmission electron microscope (TEM) image taken at high magnification showing CNFs in CNF–SMPU composite. (c) TEM image of SiC–SMPU composite with 5 wt% filler content indicating the coexistence of filler agglomerates and individually dispersed SiC particles.

3.2. Analysis of filler–polymer interactions using fluorescence emission spectroscopy

In an effort to identify the origins of the peaks observed in the fluorescence emission spectra of SMPU, we first analyzed the fluorescence emission spectra of solid SMPU and dilute solution of SMPU in dichloromethane (DCM) with a concentration of about 1 g L^{-1} and compared them with those of the dilute solutions of *N*-methyl urethane and phenyl urethane in DCM also with a concentration of about 1 g L^{-1}. These spectra are

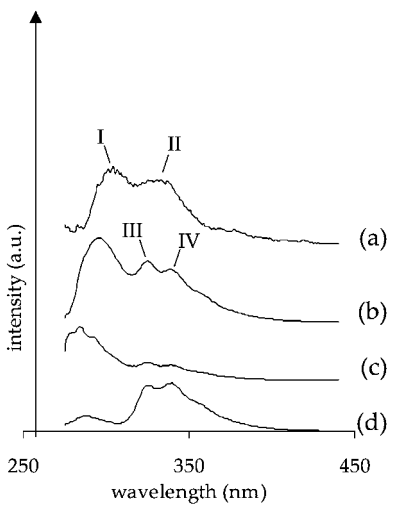

Fig. 3 Fluorescence emission spectra of compounds. Curve (a) solid SMPU, curve (b) dilute SMPU solution in DCM, curve (c) dilute *N*-methyl urethane solution in DCM and curve (d) dilute phenyl urethane solution in DCM. All spectra were taken at room temperature. The concentration of dilute solutions was about 1 g L^{-1}.

presented in Fig. 3. Note that the fluorescence emission spectra of dilute solutions usually exhibit higher resolution and yield sharper peaks due to the reduced concentration of quencher.[20]

The fluorescence spectrum of solid SMPU revealed the presence of two significant peaks identified as peaks I and II in Fig. 3, curve (a). The inspection of emission spectra of dilute solutions of SMPU, *N*-methyl urethane, and phenyl urethane in DCM indicated, however, that peak II was indeed an amalgamated peak of two distinct peaks (peaks III and IV) (Fig. 3, curve (b)). It appeared that peaks III and IV were not present in the emission spectrum of solid SMPU due to lower resolution associated with solid samples. A lower resolution in this case originated from quenching processes, or from the formation of an excimer or an exciplex.[21]

The analysis of emission spectra of the model analog compounds further revealed significant insight about the origin of the emission peaks in SMPU. Recall that *N*-methyl urethane and phenyl urethane were selected to represent the hard segments of SMPU.[22] By comparing the peak locations in Fig. 3 curve (c) with those in Fig. 3 curves (a) and (b), we attribute peak I to urethane groups in SMPU hard segments. The fluorescence emission spectra of SMPU and *N*-methyl urethane both contained peak I. The origins of peaks III and IV, and the resulting composite peak II can be attributed to the presence of aromatic groups in SMPU hard segments, for example, the aromatic rings in MDI. The emission spectra of phenyl urethane (Fig. 3, curve (d)) and SMPU (Fig. 3, curves (a) and (b)) both contained peak II. The spectra presented in Fig. 3 also suggest that the fluorescence emission of SMPU mostly originated from the hard segments, and the contribution of PCL-diol was less significant.

The fluorescence emission spectra of SMPU and its composites in the solid state at room temperature are compared in Fig. 4a–f. Note that the filler particles themselves did not show significant fluorescence emission. The intensity of peak I diminished significantly in composites of organoclay, CB, and ox-CNF, although peak II remained relatively unchanged (Fig. 4). The reduction in the intensity of emission spectra in the presence of fillers, defined as quenching, might have resulted from the energy transfer between the electrons of the excited molecules and the particles with further non-emissive relaxation.[23] In this context, recall that peak I mostly originated from the urethane groups in the hard segments of SMPU. Therefore, reduction in the intensity of peak I can be attributed to strong interactions between urethane groups and organoclay, CB, or ox-CNF particles. One might be interested in further details of interactions between clay particles and SMPU chains beyond what was stated above. Specifically, one may ask if the interactions of urethane linkages took place with the organic modifiers of the clay used in the study or if the soft segments of SMPU chains also participated in interactions with clay. Unfortunately, the interactions between SMPU and polar and non-polar organic modifiers on different clay particles[24] could not be resolved *via* the use of fluorescence emission spectroscopy, as discussed elsewhere.[25] Interestingly, the fluorescence emission spectra of ox-CNF and CB composites did not provide any evidence of interactions between the π-electrons located in the aromatic rings of the SMPU hard segments and the π-electrons, present in abundance in the graphene sheets of CB and ox-CNF due to their graphitic nature.[26] This was rather surprising since π–π interactions have been

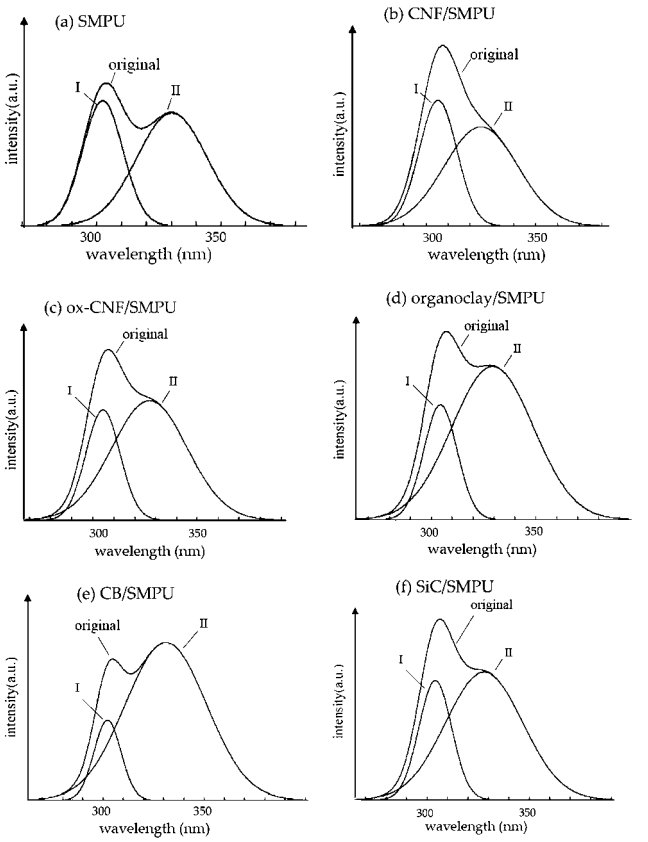

Fig. 4 Fluorescence emission spectra of SMPU composites taken at room temperature. (a) pristine SMPU, (b) CNF–SMPU, (c) ox-CNF–SMPU, (d) organoclay–SMPU, (e) CB–SMPU and (f) SiC–SMPU. Note the significant reduction in the intensity of peak I in composites of ox-CNF, CB, and organoclay. Peak I was located at around 305 nm, whereas peak II was located at around 330 nm. Each composite contained 1 wt% filler.

widely identified *via* quenching of fluorescence emission.[27] We believe that the absence of this quenching in our study resulted from the non-planar, rigid structure of SMPU hard segments.[28]

Prior research established that urethane groups and phenyl rings in hard segments can remain in different planes with different inclinations[22,29] (Fig. 5). These features of the proposed structure of hard segments can be summarized as follows:[29] (i) the phenyl groups of MDI remain mutually perpendicular to each other, (ii) the central bridge formed by (C_6H_4)–CH_2–(C_6H_4) group has an angle of 115.3°, (iii) the phenyl groups are inclined respectively at 75.1° and 34.7° to the plane of the central bridge, (iv) the urethane groups are planar, and (v) the inclinations of the urethane planes to their respective phenyl groups are 36.1° and 10.5°. As the urethane groups are highly polar, the resulting polar–polar interactions between urethane groups and polar functional groups on ox-CNF and CB particles can be stronger than the non-polar π–π interactions between the phenyl rings and the graphitic lattice of ox-CNF and CB particles. Accordingly, one may anticipate much closer positioning of urethane groups to ox-CNF and CB particle surfaces. However, such a closer positioning of urethane groups also pushes away the phenyl rings from the vicinity of ox-CNF and CB surfaces. In view of the proposed structure presented in Fig. 5, the average

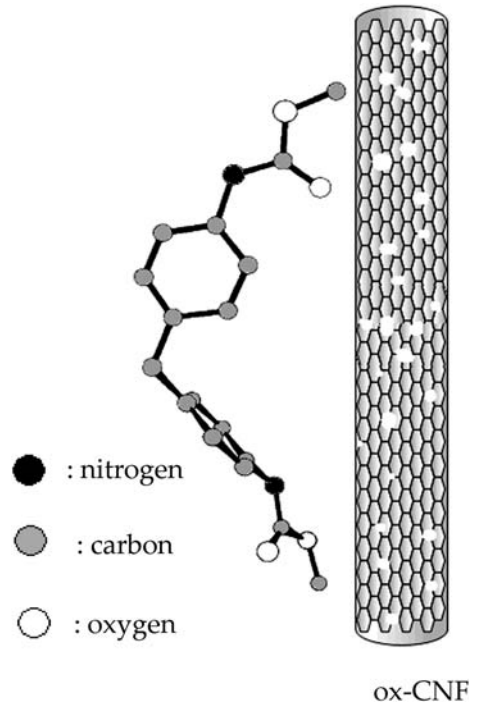

Fig. 5 Schematic representation of SMPU hard segments (CH_3–O–(CO)–NH–(C_6H_4)–CH_2–(C_6H_4)–NH–(CO)–CH_3) positioned in the proximity of ox-CNF particles. The urethane groups are placed closer to the ox-CNF particle surface due to non-covalent interactions. Consequently, phenyl rings are placed relatively away from ox-CNF particles. The schematic is not to scale. The atoms are color coded as follows: gray: carbon, black: nitrogen, white: oxygen. The proposed structure of hard segments was reprinted with permission from ref. 22.

distance of the phenyl groups from the ox-CNF and CB surfaces can be 1–2 Å higher than that of the urethane groups. Note that quenching of fluorescence emission is sensitive to the distance between the excited molecule and the quencher. The maximum distance which can still provide quenching is only about 3–4 Å.[30] Thus, even a relatively small increase in the distance between the phenyl rings and ox-CNF and CB particle surface as a consequence of much closer position of the urethane groups can prevent quenching of fluorescence emission from the phenyl rings.

It is worth mentioning here that the fluorescence emission results presented thus far did not exclude the possibility of other types of filler–polymer interactions. One may argue, for example, about the potential non-covalent interactions of urethane groups with the π-electrons located on the surfaces of CNF and ox-CNF.[31] Although these interactions are quite possible, they are much weaker compared to polar, non-covalent interactions.[31]

3.3. The relationship between the favorable filler–polymer interactions and shape memory properties

The reduced soft segment crystallinity in composites is presented in Fig. 6 as a function of the ratio of the areas under the peaks I (A_I) and II (A_{II}) obtained from fluorescence emission spectroscopy results (Fig. 4). A close correlation between the ratio A_I/A_{II} and soft segment crystallinity is apparent in Fig. 6. Note that smaller values of A_I/A_{II} represent stronger filler–polymer

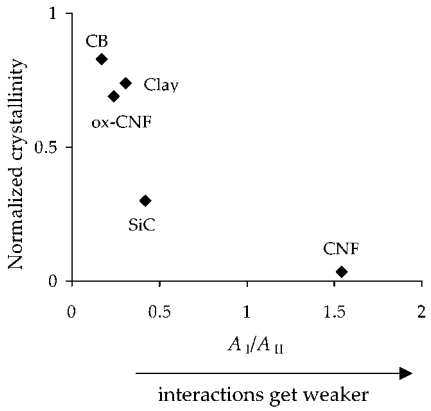

Fig. 6 The relationship between soft segment crystallinity and the ratio of the areas under the peaks I (A_I) and II (A_{II}) observed in the fluorescence emission spectra of the composites. Normalized soft segment crystallinity values were obtained after dividing the value of soft segment crystallinity of the specific composite by that of the pristine SMPU. All composites contained 1 wt% filler particles. Note that a lower value of A_I/A_{II} indicates stronger non-covalent interactions between the filler and SMPU. An inverse correlation between the soft segment crystallinity and the value of A_I/A_{II} is evident. The soft segment crystallinity values were taken from our previous reports (ref. 4 and 12).

interactions. The extent of reduction of soft segment crystallinity was more significant in composites of CNF and SiC. Note that the ratio of the peak areas did not reduce much in composites of CNF, indicating the absence of significant non-covalent interactions.

The shape memory properties, including shape fixity (SF) (Fig. 7) of composites filled with SiC and CNF were previously

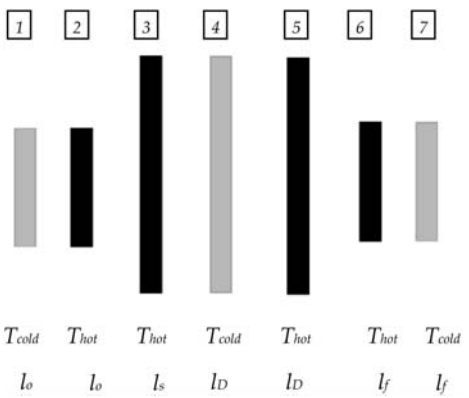

Fig. 7 Schematic of typical specimen shapes during shape memory cycle. (1) Undeformed specimen of length l_o is initially kept at a temperature (T_{cold}) which is lower than the melting point of the soft segments (T_m). (2) Specimen at a temperature above T_m (T_{hot}). (3) Specimen is deformed to length l_s. (4) Specimen is cooled down to below T_m (T_{cold}) while keeping the constraining stress in place. Constraining stress is removed after finishing the cooling. Specimen length decreased to l_D due to small instantaneous recovery. (5) Specimen is heated to above T_m (T_{hot}). (6) Specimen recovers its original shape. Note that actual specimen assumes both the shapes 4 and 5 simultaneously in real shape memory cycle. Specimen length is l_f which is close to l_o. Shape fixity is defined as the level of deformation that may be fixed upon rapid cooling of the deformed material to room temperature and its value could be computed from the sample lengths: $SF = (l_D - l_o)/(l_s - l_o)$. (7) Recovered specimen cooled down to T_{cold}.

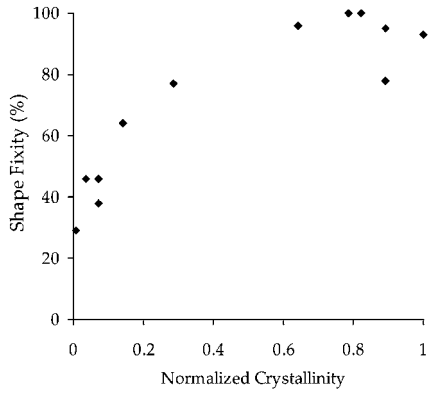

Fig. 8 The experimental data on the relationship between SF and the extent of soft segment crystallinity of SMPU composites filled with organoclay, CNF, ox-CNF, SiC, and CB. Experimental data (filled squares) were taken from previous reports.[4,12] Normalized soft segment crystallinity values were determined by dividing the value of soft segment crystallinity of the specific composite by that of the pristine SMPU.

observed to be inferior to pristine SMPU.[4] This was attributed to a reduction of soft segment crystallinity. It was noted earlier that an adequate amount of soft segment crystallinity is required for desired shape memory performance and for preserving the residual orientation of chains and chain segments in the deformed state.[2] Experimental data on crystallinity and SF of SMPU composites taken from previous reports[4,12] are presented in Fig. 8 which reveal a close correlation between SF and extent of soft segment crystallinity.

One may raise a question on the validity of correlation between fluorescence emission spectroscopy results and the extent of soft segment crystallinity. Recall that fluorescence spectroscopy data presented in Fig. 4 indicated much stronger non-covalent interactions of urethane hard segments with filler particles. The evidence of possible non-covalent bonds between the soft segments and filler particles could not be detected *via* fluorescence emission spectroscopy due to the absence of fluorescence emission from the soft segments. However, as hard segments and soft segments of SMPU are parts of the same polymer chains, the interactions between hard segments and fillers can also influence the soft segments. As outlined in Fig. 6, relating fluorescence emission spectroscopy data to soft segment crystallinity, and in this context, to the shape memory properties, yielded a very useful correlation. Especially, in composites of ox-CNF, CB, and organoclay, polar–polar interactions at filler surfaces with SMPU may have promoted adsorption of polymer chains on the filler surface, which in turn promoted favorable chain conformations and thus led to higher rates of nucleation and soft segment crystallization.[12] In the cases of CNF and SiC particles, non-attractive surfaces of SMPU chains may have prevented effective nucleation and hence reduced the degree of soft segment crystallinity.[12] Molecular dynamics simulation studies predicted depletion of polymer concentration in the vicinity of non-attractive surfaces[32] which can potentially diminish the extent of nucleation.

The close correlation seen in Fig. 8 between experimental data on shape fixity and soft segment crystallinity can be interpreted qualitatively using a thermodynamic model as follows. The shape memory function is critically dependent on the residual orientation of the stretched polymer chains.[33] The oriented polymer chains in deformed specimens facilitate shape recovery by entropic elasticity of the polymer.[34,35] In this context, we define the locked chains (or the chain segments) as the ones oriented, for example, by stretching and kept in highly oriented state by crystallization.[2] Low values of crystallinity in the stretched specimen give birth to 'unlocked' chains which are responsible for immediate shrinkage of the specimen upon unloading. Therefore, unlocked chains do not participate in the shape recovery process. The creation of 'locked' chain segments and their impact on shape memory properties can be analyzed using expressions of entropic elasticity of deformed polymer networks. Shape recovery of SMPs is governed by the change (ΔA) in the value of Helmholtz free energy (A). Note that thermodynamic expressions for ΔA and the change in entropy of deformed polymer networks are derived assuming Gaussian polymer chains.[36] It is widely known that polyurethanes and other phase separated block-copolymers do not follow Gaussian statistics.[37] Nevertheless, the predictions of the existing thermodynamic models can be used for qualitative interpretation of shape memory properties of SMPU. In this context, note that recovery stress is a direct function of ΔA, which in turn is related to stretching ratio, λ. The value of ΔA is obtained from the change in internal energy (ΔU) and the change in entropy (ΔS), as follows:

$$\Delta A = \Delta U - T\Delta S \tag{1}$$

In an isothermal process, the contribution of ΔU to ΔA is negligible. Therefore, the deformation and recovery of polymers originate from entropic elasticity. In typical non-isothermal shape memory cycle (Fig. 7), the contribution of ΔU can also be safely omitted. SMPs usually operate over a narrow temperature interval. For example, the shape memory cycle considered in this work covered a temperature range from 25 °C to 60 °C.

For an amorphous Gaussian elastomer, ΔA can be expressed according to the classical Kuhn–Treloar theory,[38,39] as follows:

$$\Delta A = \frac{RT}{2}\left(\lambda^2 + \frac{2}{\lambda} - 3\right) \tag{2}$$

In eqn (2), R is the gas constant, T is the absolute temperature, and λ is the stretching ratio. One might easily infer from eqn (2) that ΔA is zero for steps where there is no deformation ($\lambda = 1$). Similarly, ΔA for steps 3 and 5 in Fig. 7 can be obtained from eqn (2), by substituting T with T_{hot}:

$$\Delta A_3 = \frac{RT_{hot}}{2}\left(\lambda^2 + \frac{2}{\lambda} - 3\right) \tag{3}$$

$$\Delta A_5 = \frac{RT_{hot}}{2}\left(\lambda^2 + \frac{2}{\lambda} - 3\right) \tag{4}$$

In several polymers, the values of ΔA_3 and ΔA_5 may differ significantly, as polymer chains relax during cooling of the stretched specimen.

The analysis of ΔA of step 4 (Fig. 7) needs more attention due to crystallization of the deformed chains upon cooling. Flory[40] suggested a model to capture the strain-induced crystallization of elongated polymer networks by analyzing the changes in ΔA. He

assumed that crystallization strictly occurred after deformation. Note that SMPU was deformed at above the melting point of the crystals and hence crystallization occurred after the polymer was elongated to the final length which is reminiscent of Flory's strain-induced crystallization theory.[40] Flory also assumed that crystallization created new surfaces in the form of crystal lamellae and hence crystallization would use a certain portion of the available free energy induced by deformation. Thus, crystallization of a deformed elastomer counter-balanced the ΔA induced by deformation and hence reduced the extent of extractable work from the deformed elastomer in the form of instantaneous recovery. In view of this, ΔA of step 4 can be expressed as:

$$\Delta A_4 = \sigma_{em} - N\omega\Delta G_\mu + \frac{RT_{cold}}{2(1-\omega)}\left(\lambda^2 + \frac{2}{\lambda} + 3N\omega^2 - 2\lambda\omega\left[\frac{6N}{\pi}\right]^{\frac{1}{2}}\right) - \frac{3RT_{cold}}{2} \quad (5)$$

In eqn (5), σ_{em} stands for the free energy of the interface between the crystalline and amorphous sections of the chain, ω is the degree of crystallinity, ΔG_μ is the free energy of fusion of a crystalline chain segment, λ is the stretching ratio, and N stands for the number of links in the polymer chain.[41,42]

Note that an equilibrium level of crystallinity should depend on the specific system and kinetic conditions, such as the cooling rate, and in turn should define shape fixity (SF). As the degree of crystallinity approaches its equilibrium value ($\omega = \omega_{eq}$), the value of ΔA also approaches its equilibrium value of ΔA_{eq}. Approaching an equilibrium crystallinity implies that the deformed shape is stable at T_{cold} corresponding to the state of 100% SF. In addition, in some cases, crystallinity fails to approach the equilibrium value, such as in the presence of several nanoscopic fillers as we observed previously.[4] Such an imbalance in the value of ΔA induces an instantaneous shape recovery in the material, and results in reduced shape fixity and SM properties.[4] Note that high shape fixity is the first requirement to obtain strong shape memory properties since other performance parameters, such as recovery ratio and recovery stress are also dependent on the value of SF. SF can be approximated as follows:

$$SF \approx 1 - \frac{|\Delta A_4 - \Delta A_{4eq}|}{|\Delta A_{eq} - \Delta A_{40}|} \quad (6)$$

$$\Delta A_{4eq} = [\Delta A_4]_{\omega=\omega eq} \quad (7)$$

$$\Delta A_{40} = [\Delta A_4]_{\omega=0} \quad (8)$$

Eqn (6) implies that SF should assume the value of 100% if the soft segment crystallinity approaches its equilibrium value. In the absence of soft segment crystallinity, SF should assume a value of zero.

The predictions of eqn (6) for the relationship between SF and the extent of crystallinity are presented in Fig. 9. The predictions of eqn (6) were calculated using arbitrary values. Note that the exact values of predictions of eqn (6) would vary with the selection of parameters. Often, the exact values of the model parameters for any given polymer network are hard, if not impossible, to determine. However, the overall trend of the predicted curve does not change significantly with selection of parameters. A close relationship between the extent of crystallinity and SF is predicted by eqn (6). Experimental data on crystallinity and SF of SMPU composites taken from previous reports[4,12] were already discussed in Fig. 8. It is seen that the trend of the model in Fig. 9 is similar to that of the experimental data in Fig. 8. Note that our objective was not to quantitatively compare the model predictions with experimental values. First, the mismatch between the non-Gaussian nature of polyurethanes and the Gaussian approximation made in derivation of eqn (6) is obvious. Second, the exact values of model parameters for SMPU are unknown and the values used in calculations are only representative values. Nevertheless, a qualitative comparison of Fig. 8 and 9 suggests that the unbalanced Helmholtz free energy owing to the absence of adequate crystallinity in composites contributed to reductions in SM properties.

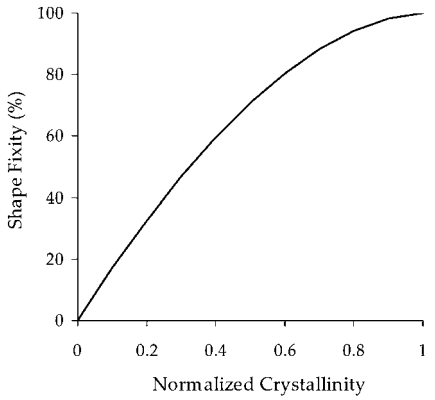

Fig. 9 The predictions of eqn (6) for the relationship between SF and the extent of soft segment crystallinity. Predicted curve was calculated using arbitrary values, although the overall trend of the predicted curve does not change significantly with selection of parameters.

4. Conclusions

The following conclusions can be drawn from this study:

(1) Fluorescence emission spectroscopy data provided evidence of polar–polar interactions between urethane groups located in the hard segments of SMPU and ox-CNF, CB, and organoclay particles. Particularly, the urethane linkages were found to participate in such interactions. It was also found that the π–π interactions between the carbonaceous particles and the aromatic rings of urethanes were relatively weaker.

(2) A close correlation was observed between the extent of non-covalent filler–matrix interactions, the degree of soft segment crystallinity, and the shape memory properties. The reduction of soft segment crystallinity caused an imbalance of Helmholtz free energy, which in turn, caused a reduction of shape memory properties.

References

1 S. Hayashi, S. Kondo, P. Kapadia and E. Ushioda, *Plast. Eng. (N. Y.)*, 1995, **51**, 29; A. Lendlein and S. Kelch, *Angew. Chem., Int. Ed.*, 2002, **41**, 2034; I. Bellin, S. Kelch, R. Langer and A. Lendlein, *Proc. Natl. Acad. Sci. U. S. A.*, 2006, **103**, 18043; A. Lendlein and

R. Langer, *Science*, 2002, **296**, 1673; I. A. Rousseau and P. T. Mather, *J. Am. Chem. Soc.*, 2003, **125**, 15300; J. Kunzelman, T. Chung, P. T. Mather and C. Weder, *J. Mater. Chem.*, 2008, **18**, 1082.
2 I. S. Gunes and S. C. Jana, *J. Nanosci. Nanotechnol.*, 2008, **8**, 1616.
3 S. Sinha Ray and M. Okamoto, *Prog. Polym. Sci.*, 2003, **28**, 1539; A. Pattanayak and S. C. Jana, *Polymer*, 2005, **46**, 3275; A. Pattanayak and S. C. Jana, *Polymer*, 2005, **46**, 3394; I. S. Gunes, F. Cao and S. C. Jana, *J. Polym. Sci., Part B: Polym. Phys.*, 2008, **46**, 1437.
4 I. S. Gunes, F. Cao and S. C. Jana, *Polymer*, 2008, **49**, 2223.
5 X. Chen, L. Wu, S. Zhou and B. You, *Polym. Int.*, 2003, **52**, 993; A. Pattanayak and S. C. Jana, *Polymer*, 2005, **46**, 5183; E. P. Plueddemann, *Silane Coupling Agents*, Plenum Press, New York, 1982; T. K. Chen, Y. I. Tien and K. H. Wei, *J. Polym. Sci., Part A: Polym. Chem.*, 1999, **37**, 2225; C. H. Dan, M. H. Lee, Y. D. Kim, B. H. Min and J. H. Kim, *Polymer*, 2006, **47**, 6718; F. Chavarria and D. R. Paul, *Polymer*, 2006, **47**, 7760.
6 G. A. Jimenez and S. C. Jana, *Carbon*, 2007, **45**, 2079.
7 G. A. Jimenez and S. C. Jana, *Proceedings of the 66th Annual Technical Meeting of Society of Plastics Engineers, Milwaukee, WI*, 2008.
8 J. L. Koenig, *Chemical Microstructure of Polymer Chains*, Wiley, New York, 1980.
9 G. W. Ewing, *Instrumental Methods of Chemical Analysis*, MacGraw-Hill, New York, 1985.
10 I. S. Gunes, C. A. Perez-Bolivar, G. A. Jimenez, F. Cao, P. Anzenbacher, Jr and S. C. Jana, *Proc. SPE ANTEC*, accepted.
11 J. E. Stamhuis and J. P. A. Loppe, *Rheol. Acta*, 1982, **21**, 103.
12 I. S. Gunes, G. A. Jimenez and S. C. Jana, *Carbon*, 2009, **47**, 981.
13 P. Anzenbacher, Jr and M. A. Palacios, *Nature Chem.*, 2009, **1**, 80.
14 W. F. Verhelst, K. G. Wolthuis, A. Voet, P. Ehrburger and J. B. Donnet, *Rubber Chem. Technol.*, 1977, **50**, 735.
15 C. D. Jung, S. C. Jana and I. S. Gunes, *Ind. Eng. Chem. Res.*, 2007, **46**, 2413.
16 T. D. Fornes, P. J. Yoon, D. L. Hunter, H. Keskkula and D. R. Paul, *Polymer*, 2002, **43**, 5915.
17 C. S. Brooks, M. A. DeCrescente and D. A. Scola, *J. Colloid Interface Sci.*, 1968, **27**, 772.
18 B. A. Higgins, PhD Thesis, The University of Akron, 2006.
19 G. A. Jimenez and S. C. Jana, *Compos. Part A: Appl. Sci. Manuf.*, 2007, **38**, 983.
20 K. H. Kim and W. H. Jo, *Macromolecules*, 2007, **40**, 3708.
21 V. B. Biteman, O. A. Gunder, I. B. Petrova and V. G. Senchishin, *J. Appl. Spectrosc.*, 1980, **33**, 1134.
22 J. Blackwell and K. H. Gardner, *Polymer*, 1979, **20**, 13.
23 M. R. Kagan and R. L. McCreery, *Anal. Chem.*, 1994, **66**, 4159.
24 H. van Olphen, *An Introduction to Clay Colloid Chemistry*, Wiley, New York, 1977, pp. 173–174.
25 F. Cao, I. S. Gunes, C. Perez-Bolivar, P. Anzenbacher, Jr. and S. C. Jana, *Proc. SPE ANTEC*, accepted.
26 C. C. White, K. B. Migler and W. L. Wu, *Polym. Eng. Sci.*, 2001, **41**, 1497.
27 J. S. Yang and T. M. Swager, *J. Am. Chem. Soc.*, 1998, **120**, 11864.
28 J. Blackwell, J. R. Quay, M. R. Nagarajan, L. Born and H. Hespe, *J. Polym. Sci., Polym. Phys. Ed.*, 1984, **22**, 1247.
29 J. Blackwell and M. R. Nagarajan, *Polymer*, 1981, **22**, 202.
30 H. Odani, *Bull. Inst. Chem. Res., Kyoto Univ.*, 1973, **51**, 351.
31 F. C. Wang, M. Feve, T. M. Lam and J. P. Pascault, *J. Polym. Sci., Part B: Polym. Phys.*, 1994, **32**, 1305.
32 C. M. Marques and J. F. Joanny, *Macromolecules*, 1990, **23**, 268.
33 G. Barot, I. J. Rao and K. R. Rajagopal, *Int. J. Eng. Sci.*, 2008, **46**, 325.
34 C. Liu, H. Qin and P. T. Mather, *J. Mater. Chem.*, 2007, **17**, 1543.
35 R. A. Weiss, E. Izzo and S. Mandelbaum, *Macromolecules*, 2008, **41**, 2978.
36 B. Erman and J. E. Mark, *Structures and Properties of Rubberlike Networks*, Oxford University Press, New York, 1997.
37 R. Bonart, *Polymer*, 1979, **20**, 1389.
38 W. Kuhn, *J. Polym. Sci.*, 1946, **1**, 380.
39 L. R. G. Treloar, *Trans. Faraday Soc.*, 1946, **42**, 77.
40 P. J. Flory, *J. Chem. Phys.*, 1947, **15**, 397.
41 R. J. Gaylord and D. J. Lohse, *Polym. Eng. Sci.*, 1976, **16**, 163.
42 R. J. Gaylord, *J. Polym. Sci., Polym. Phys. Ed.*, 1976, **14**, 1827.

